DALTON
FULL PAPER

Constrained ferromagnetic coupling in dinuclear $\mu_{1,3}$-azido nickel(II) cryptate compounds. Crystal structure and magnetic behaviour of $[Ni_2(L1)(N_3)(H_2O)][CF_3SO_3]_3\cdot 2H_2O\cdot EtOH$ $\{L1 = N[(CH_2)_2NHCH_2(C_6H_4\text{-}m)CH_2NH(CH_2)_2]_3N\}$ †

Albert Escuer,[a] Charles J. Harding,[b] Yann Dussart,[b,c] Jane Nelson,[b,c] Vickie McKee[c] and Ramon Vicente[a]

[a] *Departament de Química Inorgànica, Universitat de Barcelona, Diagonal, 647. 08028-Barcelona, Spain*
[b] *Department of Chemistry, Open University, Milton Keynes, UK MK7 6AA*
[c] *School of Chemistry, Queen's University, Belfast, UK BT9 5AG*

Received 5th August 1998, Accepted 30th October 1998

The new dinuclear compounds $[Ni_2(L1)(N_3)(H_2O)][CF_3SO_3]_3\cdot 4H_2O$ **1**, $[Ni_2(L1)(N_3)][ClO_4]_3\cdot MeCN\cdot 2H_2O$ **2,** $[Co_2(L1)(N_3)][ClO_4]_3\cdot H_2O$ **3**, and $[Mn_2(L2)(N_3)][CF_3SO_3]_3$ **4** have been prepared $\{L1 = N[(CH_2)_2NHCH_2(C_6H_4\text{-}m)CH_2NH(CH_2)_2]_3N$; $L2 = N[(CH_2)_2NHCH_2(C_6H_4\text{-}p)CH_2NH(CH_2)_2]_3N\}$. The crystal structure of $[Ni_2(L1)(N_3)(H_2O)][CF_3SO_3]_3\cdot 2H_2O\cdot EtOH$: has been determined. From magnetic measurements **1** and **2** show ferromagnetic coupling, whereas **3** and **4** show antiferromagnetic coupling. The best fit parameters are: $2J = 11.82$ cm^{-1}, $g = 2.13$, $D = 0.096$ cm^{-1} and $2z'J' = -0.72$ cm^{-1} for **1**, $2J = 7.72$ cm^{-1}, $g = 2.12$, $D = -2.38$ cm^{-1} and $2z'J' = -0.95$ cm^{-1} for **2**, $2J = -4.1$ cm^{-1}, $g = 2.11$ for **3**, and $2J = -12.1$ cm^{-1}, $g = 1.98$ for **4**. The magnetic results can be correlated with those predicted on the basis of an earlier model.

Introduction

The superexchange pathway through end-to-end single azido bridges between nickel(II) ions has been widely studied during the past few years, and a model[1,2] proposed in which the antiferromagnetic component (J_{AF}) of the coupling constant J was successfully correlated with the bond parameters, mainly the Ni–N–N bond angles and the Ni–N–N–N–Ni torsion angle, which for the linear azide bridge is based on the terminal nitrogen atoms of azide and the nickel atoms. According to this model, with a Ni–N–N–N–Ni torsion angle of 0°, the strongest antiferromagnetic coupling is expected for Ni–N–N angles near 110°. For larger Ni–N–N angles the J parameter must decrease quickly and indeed for high values of this angle (155–180°) ferromagnetic behavior is to be expected. Increasing the Ni–N–N–N–Ni torsion angle for a fixed Ni–N–N angle decreases the $-J$ value, the strongest antiferromagnetic coupling being expected for a Ni–N–N–N–Ni torsion angle equal to 0° for each Ni–N–N angle.

The same model has also been applied recently[3] to analyse the superexchange pathway through end-to-end azido bridges between manganese(II) ions. In this case, an end-to-end azido bridge between two manganese(II) ions for the entire set of Mn–N–N and Mn–N–N–N–Mn angles is always expected to produce a significant antiferromagnetic coupling.

The applicability of this model has been demonstrated[1–5] for a number of compounds of nickel(II) and manganese(II) with different M–N–N bond angles and M–N–N–N–M torsion angles. It offers a convenient description of the superexchange pathway and a good approximation to the magnitude of the J values. Our 1993 prediction states "... azido bridges with high Ni–N–N bond angles are experimentally improbable"[1] and indeed until now the region of high Ni–N–N angles has not been accessible. However, as always in Chemistry, the improbable is not impossible. Applying a strategy of using dinuclear cryptates as hosts for anionic guests it becomes relatively easy to constrain the azido ligand to adopt high Ni–N–N bond angles in the resulting cascade[6] complexes. A range of such dinuclear cryptates exists[7–9] where steric constraint confers near linearity on a M–NNN–M assembly, once azide has been co-ordinated in cascade fashion. Each transition ion is co-ordinated by an N_4 donor set, with the three secondary amino groups usually imposing trigonal geometry. The resulting co-ordinative unsaturation allows the incorporation of small bidentate bridging ligands. Flexibility of the cryptate enables the internuclear distance between the transition ions to vary, for example between 4 and 6 Å for dicopper complexes of ligand L1, so that 1-, 2- or 3-atom bridges may be incorporated.[7–10] The ellipsoidal shape of the cryptands favours a linear bridging mode. For a series of cascade complexes of azide-bridged dicopper cryptates this linearity has been demonstrated by characteristic spectroscopic signatures and recently by a crystal structure determination.[11]

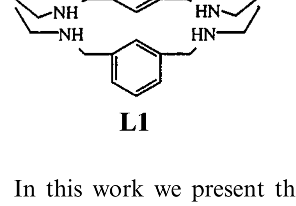

L1

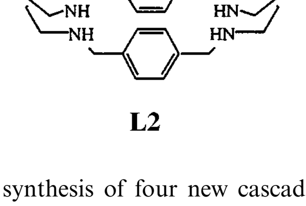

L2

In this work we present the synthesis of four new cascade complexes with the azido bridge: $[Ni_2(L1)(N_3)(H_2O)][CF_3SO_3]_3\cdot 4H_2O$ **1**, $[Ni_2(L1)(N_3)][ClO_4]_3\cdot MeCN\cdot 2H_2O$ **2,** $[Co_2(L1)(N_3)][ClO_4]_3\cdot H_2O$ **3** and $[Mn_2(L2)(N_3)][CF_3SO_3]_3$ **4,** where L1

---

† Supplementary data available: magnetic and powder diffraction data. For direct electronic access see http://www.rsc.org/suppdata/dt/1999/223/, otherwise available from BLDSC (No. SUP 57458, 8 pp.) or the RSC Library. See Instructions for Authors, 1999, Issue 1 (http://www.rsc.org/dalton).

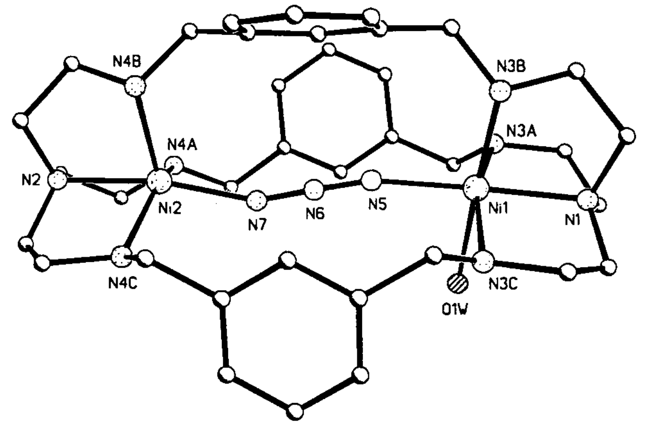

Fig. 1 Structure of the cation of $[Ni_2(L1)(N_3)(H_2O)]^{3+}$ **1a** with atom labelling scheme.

and L2 are the ligands. For one of the dinickel complexes **1**, when crystallised as $[Ni_2(L1)(N_3)(H_2O)][CF_3SO_3]_3{\cdot}2H_2O{\cdot}EtOH$ **1a**, it was possible to solve the crystal structure. In this series of azide-bridged dinuclear complexes $[M_2(N_3)L1]^{3+}$ (M = Mn, Fe, Co, Ni or Cu) the magnetic behaviour shows the net transition of antiferromagnetic to ferromagnetic exchange as predicted by the decrease in the J_{AF} component of our model.[1,2]

Results and discussion

Our previous experience with these systems led us to expect properties which we have come to recognise[7–10] as characteristic of collinear M–NNN–M disposition where a single azido ligand is co-ordinated within the cryptate host. The anomalously high $\nu_{asym}(N_3)$ infrared absorption frequency (*ca.* 2200 cm^{-1}) seen in the complexes examined here strengthens that expectation. We believe that this high frequency derives from the mechanical effect of adjacent bond interaction[9,12] *i.e.* of (N–N) bond stretch–(M–N) bond stretch correlation in the strongly coupled collinear M–NNN–M oscillator. X-Ray crystallographic results[11] confirm the basically collinear nature of the M–NNN–M assembly in the dicopper complex **5**, $[Cu_2(L1)(N_3)][ClO_4]_3{\cdot}2H_2O$. Comparison of the X-ray powder diffraction patterns now shows that the diiron complex[13] **6**, $[Fe_2(L1)(N_3)][ClO_4]_3{\cdot}2H_2O$, is isostructural with this dicopper complex (see SUP 57458). We now report the structure of the dinickel complex **1a**, which is found to contain the same nearly collinear M–NNN–M assembly.

Structure of $[Ni_2(L1)(N_3)(H_2O)][CF_3SO_3]_3{\cdot}2H_2O{\cdot}EtOH$

The $[Ni_2(L1)(N_3)(H_2O)]^{3+}$ cation contains a 1,3-azido bridge linking two nickel ions which are 6.270(1) Å apart (Fig. 1); selected bond lengths and angles are listed in Table 1. The bridge is not quite linear, the Ni–N–N angles being 165.8(5) and 157.6(5) for Ni(1) and Ni(2), respectively. The nickel ions are each co-ordinated to the bridgehead nitrogen atom, three amine donors and the azide but Ni(1) has an additional co-ordinated water. Atom Ni(1) is, therefore, six-co-ordinated but the geometry is quite irregular with the metal ion displaced out of the tren cap towards the centre of the cryptand as is normal in these cryptates. Atom Ni(2) is five-co-ordinated, displaced from the cap, and has a geometry intermediate between square pyramidal [with N(4B) apical] and trigonal bipyramidal (with the bridgehead and the azide donors apical). The nearest atom to the "vacant" co-ordination site is O(33), a donor from one of the triflate counter ions, but this is interacting with the proton on N(4C) rather than with Ni(2) [interatomic distances 2.926(7) and 3.114(5) Å, respectively].

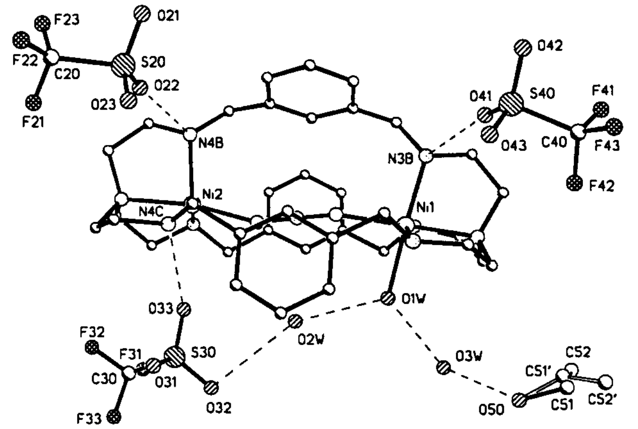

Fig. 2 Structure of the compound $[Ni_2(L1)(N_3)(H_2O)][CF_3SO_3]_3{\cdot}2H_2O{\cdot}EtOH$ **1a**, showing triflate anions and lattice solvate molecules.

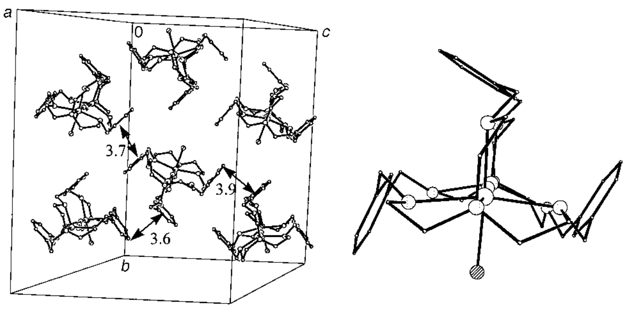

Fig. 3 The structure of compound **1a** showing π–π intermolecular interactions involving each of the three phenyl rings.

Table 1 Selected bond lengths (Å) and angles (°) for $[Ni_2(L1)(N_3)(H_2O)][CF_3SO_3]_3{\cdot}2H_2O{\cdot}EtOH$

Ni(1)–N(1)	2.083(5)	Ni(2)–N(2)	2.118(5)
Ni(1)–N(3A)	2.154(5)	Ni(2)–N(4A)	2.115(5)
Ni(1)–N(3B)	2.117(5)	Ni(2)–N(4B)	2.072(5)
Ni(1)–N(3C)	2.135(5)	Ni(2)–N(4C)	2.100(5)
Ni(1)–N(5)	2.037(5)	Ni(2)–N(7)	1.988(6)
Ni(1)–O(1W)	2.224(4)	N(5)–N(6)	1.154(7)
N(6)–N(7)	1.173(7)		
N(1)–Ni(1)–N(3A)	82.63(19)	N(4A)–Ni(2)–N(2)	82.41(19)
N(1)–Ni(1)–N(3B)	83.63(19)	N(4B)–Ni(2)–N(2)	84.2(2)
N(1)–Ni(1)–N(3C)	83.14(19)	N(4C)–Ni(2)–N(2)	82.79(19)
N(3B)–Ni(1)–N(3A)	92.33(18)	N(4B)–Ni(2)–N(4A)	107.3(2)
N(3B)–Ni(1)–N(3C)	96.51(19)	N(4B)–Ni(2)–N(4C)	104.0(2)
N(3C)–Ni(1)–N(3A)	162.30(19)	N(4C)–Ni(2)–N(4A)	143.6(2)
N(5)–Ni(1)–N(1)	177.0(2)	N(7)–Ni(2)–N(2)	169.0(2)
N(5)–Ni(1)–N(3A)	100.3(2)	N(7)–Ni(2)–N(4A)	95.6(2)
N(5)–Ni(1)–N(3B)	96.7(2)	N(7)–Ni(2)–N(4B)	106.6(2)
N(5)–Ni(1)–N(3C)	93.9(2)	N(7)–Ni(2)–N(4C)	92.7(2)
N(6)–N(5)–Ni(1)	165.8(5)	N(6)–N(7)–Ni(2)	157.6(5)
N(1)–Ni(1)–O(1W)	94.00(17)	N(5)–N(6)–N(7)	178.6(6)
N(3A)–Ni(1)–O(1W)	89.98(17)	N(3B)–Ni(1)–O(1W)	176.45(17)
N(3C)–Ni(1)–O(1W)	80.56(18)	N(5)–Ni(1)–O(1W)	85.52(18)

Table 2 Hydrogen-bonding interactions (Å)

N(3B) ··· O(41)	3.022(7)	N(4B) ··· O(22)	3.044(8)
N(4C) ··· O(33)	2.926(7)	O(31) ··· O(50)[a]	2.735(8)
O(32) ··· O(2W)	3.102(7)	O(1W) ··· O(2W)	2.788(6)
O(1W) ··· O(3W)	2.762(6)	O(3W) ··· O(50)	2.747(8)

[a] Under symmetry operation $-x, 1 - y, 1 - z$.

There is an extensive hydrogen-bonding network in the crystal lattice involving the cation, triflate anions and lattice solvate molecules (Fig. 2); hydrogen-bond distances are listed in Table 2. The carbon atoms of the ethanol solvate were disordered and refined with 50% occupancy of two alternative sites; the corre-

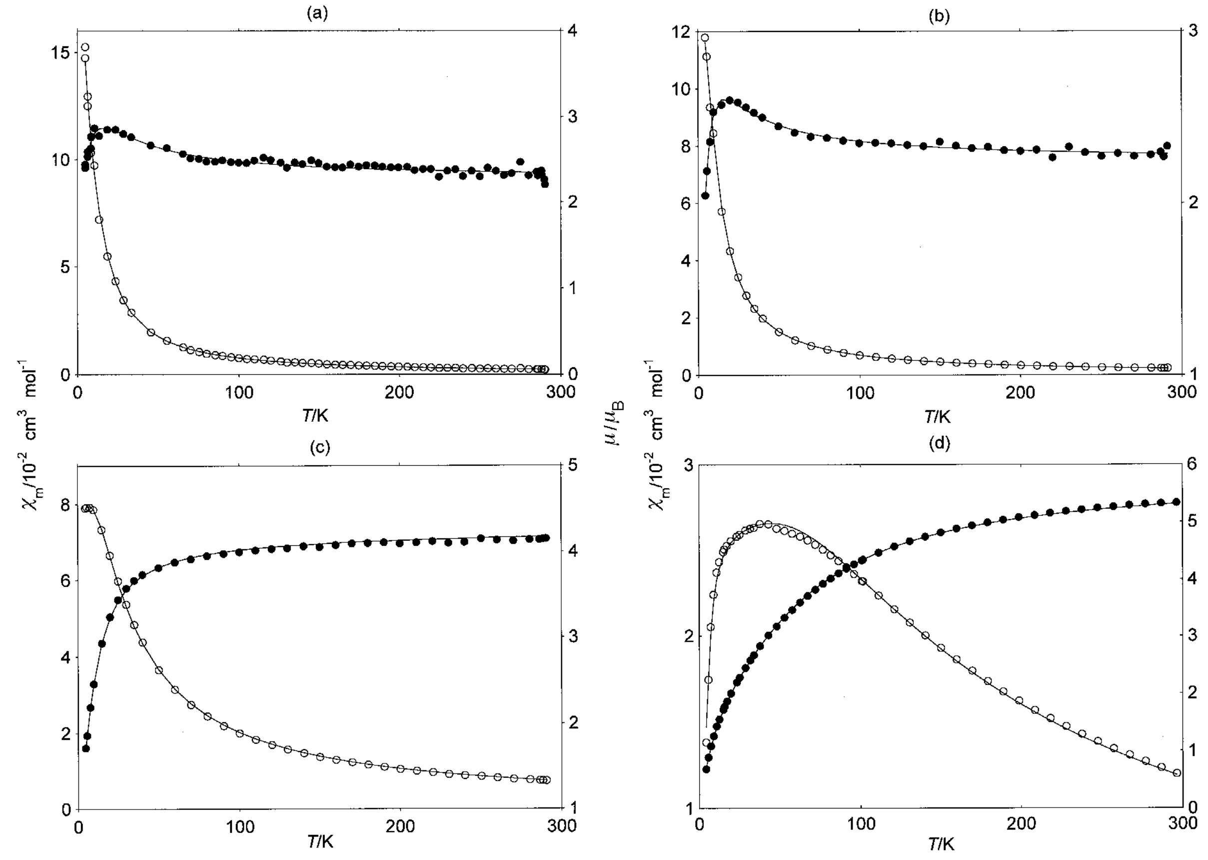

Fig. 4 Plots of χ_m (per M^{2+}) *vs.* T (○) and μ *vs.* T (●) experimental data for complexes (a) **1**, (b) **2**, (c) **3** and (d) **4**. Solid lines show the best fit obtained (see text).

sponding oxygen atom was not disordered, being anchored by hydrogen bonding to a water molecule, O(3W).

The cations show some π–π intermolecular interactions involving each of the three phenyl rings (interplanar distances of 3.6–3.9 Å), linking the cations into two-dimensional sheets (Fig. 3). The bridging azide is 2.9–3 Å from the mean plane of each ring but there is no very convincing evidence for intermolecular interaction and the geometry argues against it; the azide is not in line with the π systems.

Magnetic results

The molar magnetic susceptibilities and magnetic moments *vs.* T of complexes **1**–**4** are plotted in Fig. 4. For $[Ni_2(L1)(N_3)(H_2O)][CF_3SO_3]_3\cdot4H_2O$ **1** the χ_m value (per M^{2+}) of 2.09×10^{-3} cm^3 mol^{-1} at room temperature increases continuously when the temperature decreases, giving no maximum. The value of μ, 2.20 μ_B at room temperature, first increases with decreasing temperature, reaching a maximum of 2.85 μ_B at 20 K, and finally decreases to 2.4 μ_B at 5 K. This behaviour indicates a global ferromagnetic coupling between the nickel(II) ions with a small interdimer antiferromagnetic interaction. The compound $[Ni_2(L1)(N_3)][ClO_4]_3\cdot MeCN\cdot2H_2O$ **2** shows similar behaviour. However, for $[Co_2(L1)(N_3)][ClO_4]_3\cdot H_2O$ **3** the value of χ_m, 7.4×10^{-2} cm^3 mol^{-1} at room temperature, first increases as the temperature decreases, reaching a maximum value of 7.9×10^{-2} cm^3 mol^{-1} at 6 K. Similarly for $[Mn_2(L2)(N_3)][CF_3SO_3]_3$ **4** the value of χ_m increases from 1.2×10^{-2} cm^3 mol^{-1} at room temperature until about 40 K when it reaches a maximum of 2.7×10^{-2} cm^3 mol^{-1}. This behaviour indicates an overall antiferromagnetic coupling between the cobalt(II) ions in complex **3** and between the manganese(II) ions in **4**.

The χ_mT *vs.* T experimental data for complexes **1** and **2** were least-squares fitted [by minimising the function $R = \Sigma(\chi_m^{calc} - \chi_m^{obs})^2/\Sigma(\chi_m^{obs})^2$] by the expression of the magnetic susceptibility of Ginsberg,[14] from the Hamiltonian (1) in which

$$H = -2JS_1S_2 - D(S_{1z}^2 + S_{2z}^2) - g\beta H(S_1 + S_2) - z'J'S\langle S\rangle \quad (1)$$

J is the intradimer exchange parameter, D the single-ion zero-field splitting and $z'J'$ the quantity for effective interdimer exchange; it is assumed that $g_x = g_y = g_z = g$. The resulting χ_m expression is (2), F_1 and F' being functions of temperature,

$$\chi_m = 2Ng^2\beta^2/3k\{[F_1/(T - 4z'J'F_1)] + [2F'/(1 - 4z'J'F')]\} \quad (2)$$

zero-field splitting and the intradimer exchange parameter J. The best-fitting parameters obtained are $2J = 11.82$ cm^{-1}, $g = 2.13$, $D = 0.096$ cm^{-1} and $2z'J' = -0.72$ cm^{-1}, $R = 3.13 \times 10^{-4}$ for **1** and $2J = 7.72$ cm^{-1}, $g = 2.12$, $D = -2.38$ cm^{-1} and $2z'J' = -0.95$ cm^{-1}, $R = 5.5 \times 10^{-5}$ for **2**. The χ_mT *vs.* T experimental data for **3** and **4** were least-squares fitted by the expression of the magnetic susceptibility from the Hamiltonian $H = -2JS_1S_2$. The best-fitting parameters obtained are $2J = -4.1$ cm^{-1}, $g = 2.11$, for **3**, and $2J = -12.1$ cm^{-1}, $g = 1.98$, with $R = 0.06 \times 10^{-6}$ for **4**; it was also necessary to include a correction for a monomeric Curie-law impurity (1.8%) in the fitting of the data for **4** (see SUP 57458).

For the d^9–d^5 series of dinuclear compounds, superexchange parameters for the azide-bridged cryptates obtained in this and our previous work[7,11,13] are summarised in Table 3. These include the diiron[13] and dicopper cryptates[11] of L1. Attempts to synthesize the 1,3-azido-bridged dimanganese(II) complex of L1 were consistently unsuccessful, presumably due to the steric constraints of the cryptand cavity on the M–NNN–M assembly with these larger cations. However, the analogous L2 complex **4** contains the same collinear M–NNN–M, as judged

Table 3 Magnetic data for the dinuclear complexes $[M_2L(N_3)]X_3{\cdot}n$solv

M	Mn[a]	Fe[b]	Fe[b]	Co[a]	Ni[a]	Ni[a]	Cu[c]	Cu[c]
L	L2	L1	L1	L1	L1	L1	L1	L1
X	$CF_3SO_3^-$	$CF_3SO_3^-$	ClO_4^-	ClO_4^-	$CF_3SO_3^-$	ClO_4^-	$CF_3SO_3^-$	ClO_4^-
*n*solv	—	$2H_2O$	$2H_2O$	H_2O	$4H_2O$	$2H_2O$	—	—
$-2J$/cm^{-1}	12.1	9.0	2.6	4.1	−11.82	−7.72	−10	−15
g	1.98	2.24	2.07	2.11	2.13	2.12	2.13	2.13
$-2z'J'$/cm^{-1}					0.72	0.95		
D/cm^{-1}					0.096	−2.38		

[a] This work. [b] Ref. 13. [c] Ref. 11.

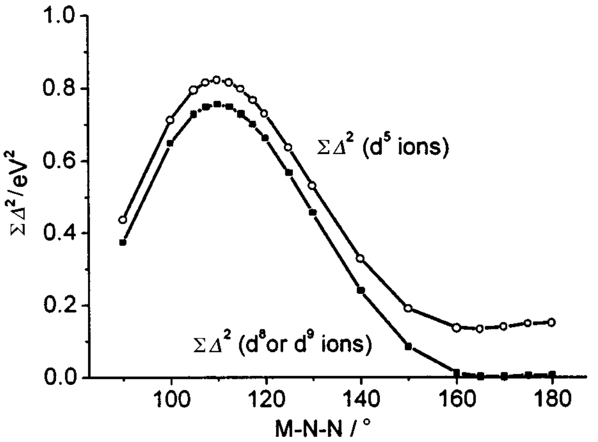

Fig. 5 Plot of $\Sigma\Delta^2$ (Δ is the gap between the corresponding antibonding MOs with the same symmetry[4,15]) which is proportional to J_{AF}, showing the negligible contribution of the antiferromagnetic component of J for d^8 or d^9 cations in contrast with the significant contribution due to the t_{2g} superexchange pathways found for d^5 cations.

Table 4 Crystallographic data for $[Ni_2(L1)(N_3)(H_2O)][CF_3SO_3]_3{\cdot}2H_2O{\cdot}EtOH$ **1a**

Formula	$C_{41}H_{66}F_9N_{11}Ni_2O_{13}S_3$
Formula weight	1305.65
Crystal symmetry	Monoclinic
Space group	$P2_1/c$
a/Å	17.5006(3)
b/Å	21.0205(4)
c/Å	16.4021(3)
β/°	115.341(1)
U/Å^3	5453.2(2)
Z	4
T/K	161(2)
D_c/g cm^{-3}	1.590
μ(Mo-Kα)/mm^{-1}	0.906
$R1$ ($I > 2\sigma I$)	0.0753
$wR2$ ($I > 2\sigma I$)	0.1550
(all data)	0.1774

by the IR criterion,[9] and thus provides a valid comparison of magnetic interactions within the azide-bridged dimanganese system.

In recent years, successful correlations of the superexchange coupling J as a function of the bond parameters, mainly bond and torsion angles related to the single end-to-end azido bridge, have been performed by means of extended-Hückel modelling.[2,4] This model uses the relationship, developed by Hoffmann and co-workers,[15] in which the antiferromagnetic component (J_{AF}) of the coupling constant (J) is proportional to the sum of the squares of the energy differences ($\Sigma\Delta^2$) between the symmetric and antisymmetric combinations of MOs. In the case of dinickel complexes these are derived from the d_{z^2} and d_{xy} orbitals. For very large (close to 180°) M–N–N bond angles the expected magnetic properties have been predicted, but until now experimental verification has not been possible. For the superexchange pathway through end-to-end single azido bridges between copper(II), d^9, and nickel(II), d^8, the cation magnetic orbitals are e_g whereas the filled t_{2g} atomic orbitals are magnetically inactive. By contrast, for d^7–d^5 cations all the e_g and t_{2g} atomic orbitals are magnetically active. From the MO analysis of the antiferromagnetic component (J_{AF}) in terms of the Hoffman formalism it was concluded that for high M–N–N values (165–180°) ferromagnetic behaviour should be expected for Cu^{II} and Ni^{II} on the basis of accidental orthogonality[1,2] between the magnetic orbitals of the cation and the HOMO of azide, whereas for d^7–d^5 ions antiferromagnetic coupling should always be dominant,[4] due to the t_{2g} superexchange pathways. A plot of $\Sigma\Delta^2$ *vs.* M–N–N bond angle, calculated from the model previously reported[4,16] for d^8 and d^5 ions, is shown in Fig. 5. Analysis of the large (M–N–N)-angle region shows that the J_{AF} component is expected to be negligible where the cation is Cu^{II} or Ni^{II}, allowing for weak ferromagnetism, whereas antiferromagnetic coupling should be found for Co^{II}, Fe^{II} or Mn^{II}. This prediction is in full accord with the experimental data listed in Table 3, demonstrating the validity of this prediction.

Conclusion

Our results further illustrate the versatility of the azido anion as mediator of magnetic interactions. In contrast to the role played by the 1,1-azido bridge at M–N–M bond angles greater than 108°,[17] the 1,3-azido bridge at large angles is shown to facilitate ferromagnetic interaction between d^8 or d^9 transition ions systems for large M–N–N bond angles. However, as the cation magnetic orbital occupancy extends beyond e_g to t_{2g} orbitals, the sense of the magnetic interaction reverses, and weak to moderate antiferromagnetic interaction is instead observed. These findings demonstrate the potential of azido bridged materials for fine-tuning of magnetic interactions, in response to bridge geometry and choice of cation.

Experimental

Syntheses

$[Ni_2(L1)(N_3)(H_2O)][CF_3SO_3]_3{\cdot}4H_2O$ 1. The ligand L1 (0.1 mmol), prepared as described elsewhere,[7] was dissolved in 5 ml EtOH and $Ni(CF_3SO_3)_2{\cdot}6H_2O$ (0.2 mmol in 2 ml MeCN) was added slowly with stirring at 25 C, before the addition of 0.1 mmol of NaN_3 dissolved in 3 drops of water and 2 ml EtOH. The solution was filtered and left to crystallise in an ether bottle. A green-blue solid was filtered off after 3 d. The sample was recrystallised from MeCN–EtOH to give X-ray quality crystals of **1a** $[Ni_2(L1)(N_3)(H_2O)][CF_3SO_3]_3{\cdot}2H_2O{\cdot}EtOH$. (Found: C, 35.7; H, 4.6; N, 11.6. $C_{39}H_{64}F_9N_{11}Ni_2O_{14}S_3$ **1** requires C, 36.2, H, 4.9; N, 11.9%); $\tilde{\nu}_{max}$/cm^{-1} (N–H) 3250, (C_{ali}–H) 2926–2876, (linear N_3) 2195, (ligand) 1445, 797, 757, 701, ($CF_3SO_3^-$) 1256, 1165 and 1031.

$[Ni_2(L1)(N_3)][ClO_4]_3{\cdot}MeCN{\cdot}2H_2O$ 2. The compound L1 (0.2 mmol) was dissolved in a mixture of EtOH (10 ml) and MeCN

(10 ml) before $Ni(ClO_4)_2{\cdot}6H_2O$ (0.4 mmol) in a mixture of EtOH (10 ml) and MeCN (10 ml) was added. The resulting blue solution was stirred for 5 min before NaN_3 (0.21 mmol) in a mixture of water (10 drops) and EtOH (4 ml) was added. The solution was stirred for 5 min before being left to evaporate for 2 h. Filtration gave a blue compound, $[Ni_2(L1)(N_3)][ClO_4]_3{\cdot}MeCN{\cdot}2H_2O$ (Found: C, 40.5; H, 5.4; N, 15.0. $C_{38}H_{61}Cl_3N_{12}Ni_2O_{14}$ requires C, 40.3, H, 5.4; N, 14.8%); $\tilde{\nu}_{max}$/cm^{-1} (N–H) 3258, (C_{ali}–H) 2926–2860, (linear N_3) 2183, (ligand) 1438, 795, 753, 700, (ClO_4^-) 1092 and 624.

$[Co_2(L1)(N_3)][ClO_4]_3{\cdot}H_2O$ 3. The compound L1 (0.2 mmol) was dissolved in a mixture of MeOH (10 ml) and EtOH (10 ml) before $Co(ClO_4)_2$ (0.4 mmol) in EtOH (20 ml) was added. The resulting turbid khaki solution was stirred for 5 min before NaN_3 (0.2 mmol) in a mixture of water (10 drops) and EtOH (4 ml) was added. The solution was stirred for 5 min before being filtered to give a deep green compound which was recrystallised in MeCN as $[Co_2(L1)(N_3)][ClO_4]_3{\cdot}H_2O$ (Found: C, 40.3; H, 5.3; N, 14.3. $C_{36}H_{56}Cl_3Co_2N_{11}O_{13}$ requires C, 40.2, H, 5.3; N, 14.3%); $\tilde{\nu}_{max}$/cm^{-1} (N–H) 3247, (C_{ali}–H) 2925–2879, (linear N_3) 2198, (ligand) 1594, 1447, 1440, 1020, 793, 757, 699, (ClO_4^-) 1092 and 623.

$[Mn_2(L2)(N_3)][CF_3SO_3]_3$ 4. The compound L2 (1 mmol) prepared as described elsewhere,[9] dissolved in EtOH (30 ml) was added to $Mn(CF_3SO_3)_2$ (0.25 mmol) in MeCN (50 ml), and finally NaN_3 (0.1 mmol) dissolved in 3 drops of water and EtOH (5 cm^3) was added with vigorous stirring. On evaporation, small crystals of pale brown product were obtained in *ca.* 60–70% yield (Found: C, 38.9; H, 4.3; N, 12.4. $C_{39}H_{54}F_9Mn_2N_{11}O_9S_3$ requires C, 39.1, H, 4.5; N, 12.9%); $\tilde{\nu}_{max}$/cm^{-1} (N–H) 3222, (C_{ali}–H) 2937 – 2857, (linear N_3) 2188, ($CF_3SO_3^-$) 1251, 1172 and 1032.

All reagents described here and in the ligand syntheses[7,9] were supplied by Aldrich Chemical Co.

Physical measurements

Variable-temperature magnetic measurements were carried out on polycrystalline samples using a pendulum type magnetometer (Manics DSM8), equipped with a helium continuous-flow cryostat working in the temperature range 300–4 K and a Drusch EAF 16UE electromagnet operating at a magnetic field of approximately 1.5 T, and with a Faraday type magnetometer (Oxford Instruments) equipped with a helium continuous-flow cryostat working in the temperature range 300–4 K and an electromagnet operating at a magnetic field of 0.8 T. Diamagnetic corrections were estimated from Pascal tables. Powder diffractometer data were collected on a Siemens D5000 powder diffractometer using Cu-Kα radiation ($\lambda = 1.54$ Å).

Infrared spectra were recorded as KBr discs at room temperature using a BioRad FTS 186 or a PE 983G spectrophotometer.

Crystal structure determination of complex 1a

Data for a crystal of dimensions 0.46 × 0.25 × 0.08 mm were collected using a Siemens SMART CCD diffractometer with Mo-Kα radiation ($\lambda = 0.71073$ Å). 27832 Reflections collected, 8939 independent ($R_{int} = 0.108$) and used in all calculations. Details are given in Table 4. Final $wR(F^2) = 0.1550$, conventional $R1 = 0.0753$ (data with $F^2 > 2\sigma$). All programs used in the structure solution and refinement are contained in the SHELXL-97 package.[18]

CCDC reference number 186/1229.

See http://www.rsc.org/suppdata/dt/1999/223/ for crystallographic files in .cif format.

Acknowledgements

This work was supported financially by Accion Integrada Hispano-Britanica HB1996–0027. We are grateful to Professor W. T. Robinson, University of Canterbury, New Zealand for access to the diffractometer.

References

1 A. Escuer, R. Vicente, J. Ribas, M. S. El Fallah, X. Solans and M. Font-Bardía, *Inorg. Chem.*, 1993, **32**, 3727.
2 A. Escuer, R. Vicente, J. Ribas, M. S. El Fallah, X. Solans and M. Font-Bardía, *Inorg. Chem.*, 1994, **33**, 1842.
3 A. Escuer, R. Vicente, M. A. S. Goher and F. Mautner, *Inorg. Chem.*, 1996, **35**, 6386.
4 A. Escuer, R. Vicente, M. S. El Fallah, X. Solans and M. Font-Bardía, *J. Chem. Soc.*, *Dalton Trans.*, 1996, 1013.
5 A. Escuer, R. Vicente, X. Solans and M. Font-Bardía, *Inorg. Chem.*, 1994, **33**, 6007.
6 J.-M. Lehn, *Pure Appl. Chem.*, 1980, **52**, 2441.
7 C. J. Harding, Q. Lu, J. F. Malone, D. J. Marrs, N. Martin, V. McKee and J. Nelson, *J. Chem. Soc.*, *Dalton Trans.*, 1995, 1739.
8 Q. Lu, J. M. Latour, C. J. Harding, N. Martin, D. J. Marrs, V. McKee and J. Nelson, *J. Chem. Soc.*, *Dalton Trans.*, 1994, 1471.
9 M. G. B. Drew, J. Hunter, D. J. Marrs, J. Nelson and C. J. Harding, *J. Chem. Soc.*, *Dalton Trans.*, 1992, 3235.
10 Q. Lu, C. J. Harding, V. McKee and J. Nelson, *J. Chem. Soc.*, *Chem. Commun.*, 1993, 1768.
11 C. J. Harding, F. E. Mabbs, E. J. MacInnes, V. McKee and J. Nelson, *J. Chem. Soc.*, *Dalton Trans.*, 1996, 3227.
12 M. G. B. Drew, P. Yates, C. J. Harding, D. McDowell, C. Stevenson, S. Raghunathan and J. Nelson, *J. Chem. Soc.*, *Dalton Trans.*, 1990, 2521.
13 F. A. Deeney, C. J. Harding, G. G. Morgan, V. McKee, J. Nelson, S. J. Teat and W. Clegg, *J. Chem. Soc.*, *Dalton Trans.*, 1998, 1837.
14 A. P. Ginsberg, *Inorg. Chem.*, 1972, **11**, 2884.
15 P. J. Hay, J. C. Thibeault and R. Hoffmann, *J. Am. Chem. Soc.*, 1975, **97**, 4884.
16 C. Mealli and D. M. Proserpio, CACAO program (Computed Aided Composition of Atomic Orbitals), *J. Chem. Educ.*, 1990, **67**, 399.
17 S. S. Tandon, L. K. Thompson, M. E. Manuel and J. N. Bridson, *Inorg. Chem.*, 1994, **33**, 5555.
18 G.M. Sheldrick, SHELXL 97, University of Göttingen, 1997.

Paper 8/06574B